https://doi.org/10.22226/2410-3535-2022-2-94-99

Annealing-induced recrystallization of iron after high pressure torsion at 80 K

K. E. Shugaev, M. V. Degtyarev, L. M. Voronova†, T. I. Chashchukhina, T. M. Gapontseva

†highpress@imp.uran.ru

M. N. Mikheev Institute of Metal Physics, UB of RAS, Yekaterinburg, 620990, Russia

Grain growth during recrystallization of pure iron with a submicrocrystalline structure formed by 5 revolutions of an anvil of high-pressure torsion deformation at cryogenic temperature (80 K) has been studied by transmission and scanning electron microscopy and durometry. Annealing at 523 K has significantly developed recrystallization (to 90% of the material volume). The average recrystallized grain size is 2 μm. The primary recrystallization has been completed after 1-h annealing at 823 K, forming grains with an average grain size of 6.5 μm. Annealing at 823 K has resulted in a large number of fine grains due to the formation of thermally activated centers of recrystallization. The grain size variability, which is characterized by the formation of grains with a size of five or more times greater than the average grain size, is observed. The average grain size has remained unchanged according to the scanning electron microscopy data, and decreased according to transmission electron microscopy data. The recrystallization texture of an axial <110> type has formed during annealing at 823 K. An increase in the annealing temperature to 923 K has increased the sharpness of the recrystallization texture. The hardness of iron has remained dependent on the true strain (distance from the sample center) after annealing at all temperatures under study.

Keywords: iron, cryogenic deformation, high pressure torsion, recrystallization, structure.

1. Introduction

High pressure torsion (HPT) deformation at cryogenic temperature results in the severe structure refinement and hardening of pure metals, such as Nb, Fe, Ti, and Ni, with melting temperatures high enough to avoid self-annealing during post-deformation aging at room temperature [1–3]. Nanostructures can form in these metals during HPT cryodeformation, and they remain in the metal structure after warming to room temperature. The high stored energy of this structure reduces the recrystallization temperature [1, 3–5]. In addition, the HPT-induced formation of microcrystallites, which are structural elements with high-angle boundaries and practically free of dislocations, makes recrystallization possible through a continuous mechanism, avoiding a nucleation stage [6–8]. Recrystallization that takes place in the deformed material at a temperature that is lower than that at which recrystallization nuclei form during thermoactivation is commonly referred to as low-temperature recrystallization [9]. Low-temperature recrystallization (at 473–573 K) in pure single-phase iron deformed by room-temperature HPT makes the boundaries and shape of the deformation-induced microcrystallites perfect [10]. As a result, a geometrically perfect recrystallized structure with submicron grain size and high thermal stability forms [11]. The formation of this recrystallized structure in iron is guaranteed by the existence of a deformation-induced uniform isotropic submicrocrystalline (SMC) structure, consisting of microcrystallites with close sizes and strongly misoriented with respect to each other. If a room-temperature deformed structure contains both microcrystallites and dislocation cells with low-angle boundaries (LAB), then recrystallization of this structure leads to the large average grain size and low thermal stability [11]. The recrystallization patterns of SMC materials have been established mainly for structures formed by room temperature deformation [11–15]. There are a limited number of papers devoted to recrystallization after cryogenic deformation [3, 5,16,17]. All researchers report a decrease in the thermal stability after cryogenic deformation due to the high stored energy. On the other hand, cryogenic deformation activates mechanical twinning, preventing the formation of a uniform isotropic SMC structure. Low-angle misorientations in the iron structure were observed [18] after cryogenic deformation up to the maximum achieved true strains.

A nonuniform structure formed by deformation can negatively affect its stability during subsequent heating. For example, severely-deformed quenched steel, in which close orientations of microcrystallites within the initial martensitic laths are preserved, experiences a catastrophic growth of individual grains upon heating [19]. Phase transformation induced by high pressure in metastable austenitic steels, which causes heterogeneity of the deformation structure, also is responsible for the development of heterogeneity during subsequent annealing [20]. The thermal stability of molybdenum deformed by different techniques (ECAP, HPT) was investigated in [8]. The authors explain the high stability of the homogeneous structure formed by HPT by the continuous static recrystallization upon annealing, in contrast to the discontinuous recrystallization that

occurs after ECAP. However, both discontinuous and continuous recrystallization features were observed in HPT-deformed nickel at room temperature upon annealing [21]. Nonsimultaneous recrystallization in niobium deformed at a cryogenic temperature was revealed in [16]. Broad size distribution of recrystallized grains was obtained in this case. How the inhomogeneity of an SMC structure formed by cryogenic deformation influences static recrystallization in iron is still an open question. Therefore, the aim of this work is to study the annealing-induced structural and hardness changes of pure iron with a SMC structure formed by HPT deformation at a cryogenic temperature.

2. Experimanral

Iron of 99.97% purity (0.003 wt.% carbon out of the total amount of impurities) was deformed by high pressure torsion at 80 K in Bridgman anvils. The anvils together with a sample was drowned into a liquid nitrogen bath placed on the press, where the deformation was carried out. A thermocouple attached to a stationary anvil was used to control the temperature. The deformation was initiated after cooling the entire block to 80 K. The samples to be deformed were 5 mm in diameter and 0.3 mm thick. The deformation was performed at a pressure of 8 GPa and a rate of 0.3 rpm. The angle of anvil rotation was 5 revolutions. The true strain was calculated by the formula from [19] taking into account the angle of anvil rotation, the distance from the sample center, and the upsetting, which depended on the distance from the sample center.

The true strain at the sample center and at distances of 1.0 and 1.5 mm from the center were 3.5, 8.2, and 8.9, respectively. The error caused by the spread in the sample thickness at the same distance from the center was $\Delta e = \pm 0.2$.

Isothermal annealing of the deformed samples was carried out at temperatures of 523 – 923 K at a step of 100 K in a vacuum (10^{-5} Pa) furnace during 1 h. Temperature fluctuations in the isothermal zone of the furnace did not exceed 5 K.

The Vickers hardness before and after annealing was measured along two mutually perpendicular sample diameters at a step of 0.25 mm and a load of 0.5 N using a PMT-3 tester. The hardness distribution over the radius of an annealed sample was found by averaging the values measured at the same radius. The hardness measurement error did not exceed 7%.

The fine structure was examined at a distance of 1.5 mm from the sample center using a JEM-200CX transmission electron microscope (TEM). The distance was estimated with an accuracy of ±0.2 mm. At least 200 measurements were made using bright-field and dark-field images in a {110}α reflection to find the sizes of microcrystallites and recrystallized grains. The recrystallized structure (grain size, grain orientation, boundary misorientation angle range, texture, recrystallized structure fraction, dislocation density) was analyzed using a QUANTA_200 Philips scanning electron microscope (SEM) equipped with an EDAX/TSL attachment for analysis of back-scattered electron diffraction (EBSD). EBSD analysis was performed at an accelerating voltage of 20 kV. The scanning step was varied from 0.1 to 0.45 μm, depending on the grain size. Prior to EBSD analysis, the samples were subjected to mechanical and electrolytic polishing in a chromic anhydride and orthophosphoric acid solution. Points with a confidence index (CI) below 0.1 [22] and grains containing less than 4 pixels were not considered. The boundaries with a misorientation angle greater than 15° were referred to as high-angle boundaries (HABs) [23]. The SEM examination was performed at a distance of 0.7 – 1.0 mm from the sample center. The average grain size was estimated by the random linear intercept method with an accuracy less than 10% (the number of intersected grains was greater than 250) [24]. The structural examinations were carried out in the plane of torsion.

3. Results and discussion

The severe plastic deformation of iron at 80 K resulted in the formation of an SMC structure with an average size of microcrystallites of 0.09 μm (Fig. 1). The structure evolution during the HPT deformation at cryogenic temperature is described in detail in [18]. This work revealed a strong dependence of the hardness of iron on the sample radius, especially at true strain $e > 5$. Therefore, to analyze the hardness as a function of the annealing temperature, we chose the data measured at the center and a distance of 0.7 – 1.0 and 1.5 mm from the sample center (r) (Fig. 2). Figure 2 shows that the hardness decreases with increasing annealing temperature. The hardness decrease at a distance of 1.5 mm from the sample center is slower than at other distances under consideration. The hardness depends on the

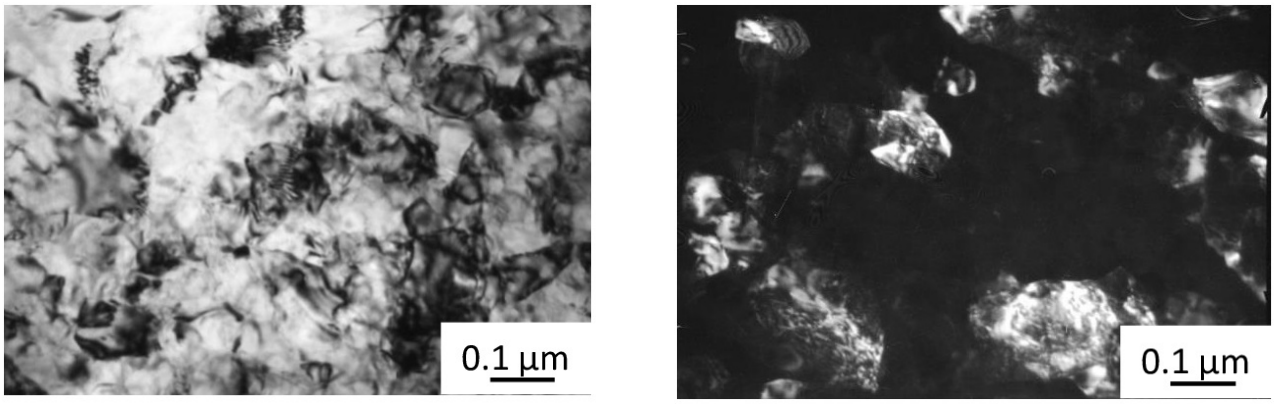

a b

Fig. 1. Structure of pure iron after HPT deformation at 80 K: bright-field image (a) and dark-field image (b) in a $(110)_\alpha$ reflection. TEM.

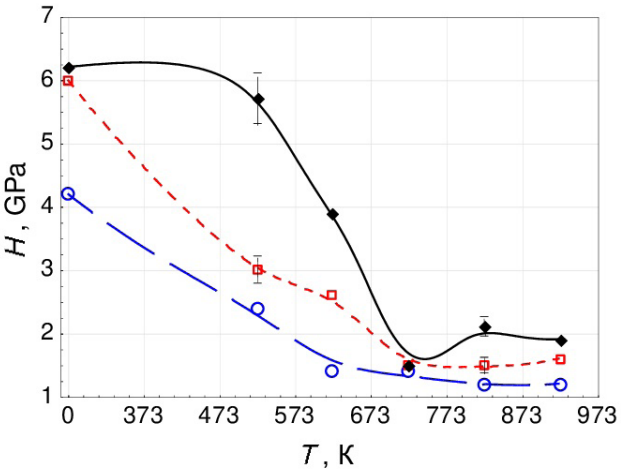

Fig. 2. (Color online) Hardness as a function of the annealing temperature at various distances from the sample center: (○) 0, (□) 0.7–1, and (◆) 1.5 mm.

sample radius (i. e., on the true strain) throughout the entire annealing temperature range. However, the differences in hardness in different parts of the sample decrease with increasing temperature. The twofold decrease in hardness at a distance of 1 mm from the center of the sample after annealing at 523 K indicates the development of recrystallization, although the hardness changes insignificantly at r=1.5 mm. Since this temperature is lower than the recrystallization temperature of a moderately deformed iron, in other words, lower than the temperature at which thermally activated recrystallization centers form (723 K according to [11, 25]), then deformation-induced microcrystallites can act as recrystallization centers.

The TEM examination confirms the onset of recrystallization at 523 K (Fig. 3 a). The figure shows that there is still a small fraction of the noncrystallized structure. According to EBSD analysis, the fraction of the recrystallized structure, which was identified on the basis of the grain orientation spread (GOS), is more than 90% (Table 1). Dislocation-free grains are considered [22, 26] to have GOS < 2.5°, whereas the formation of a substructure increases it and, in this case, GOS > 2.5°. The average recrystallized grain size reaches 2 μm. Annealing at 723 K for 1 h completes recrystallization (Fig. 3 b, Table 1). However, low-angle boundaries (LABs) remain in the structure, and the average misorientation angle does not reach the value typical of a random ensemble of grains (θ_{av} = 39° [23]). Annealing at 823 K forms finer grains (Fig. 3 c) and decreases the average grain size (Fig. 4). These structural changes are accompanied by a slight hardness increase at r=1.5 mm (Fig. 2), corresponding to the TEM examination region.

Figure 4 shows the dependence of the grain size on the annealing temperature according to SEM and TEM investigations. Two factors are responsible for the difference in the data collected by the different methods. First, TEM examination fails to observe the coarsest grains, whereas SEM examination, on the contrary, fails to detect the smallest grains. Second, the region of the SEM examination is close to the sample center, where the hardness of the material is low (Fig. 2), which corresponds to coarse recrystallized grains [27]. In iron deformed at room temperature, recrystallized grains at a distance of 1.5 mm from the center of the

Table 1. Parameters of the iron microstructure after deformation and annealing.

Parameter	Annealing temperature, K				
	523, 1 h	623, 1 h	723, 1 h	823, 1 h	923, 1 h
Fraction of HABs (>15°), %	84	85	85	78	21
Average misorientation angle, θ_{av}, deg.	34°	35°	35°	31°	11°
Kernel average misorientation, θ_{KAM}, deg.	1.4	1.1	1.1	1.1	1.4
Geometrically necessary dislocation density, ρ, $\times 10^{13}$ m^{-2}	1	1	0.6	0.7	0.4
Fraction of the recrystallized structure (GOS < 2.5°), %	96	96	99	95	60
Fraction of the area occupied by grains with sizes >5d_{av} (average grain size), %	0	0	0	8	0
Scanning step, x, μm	0.2	0.15	0.3	0.25	0.45

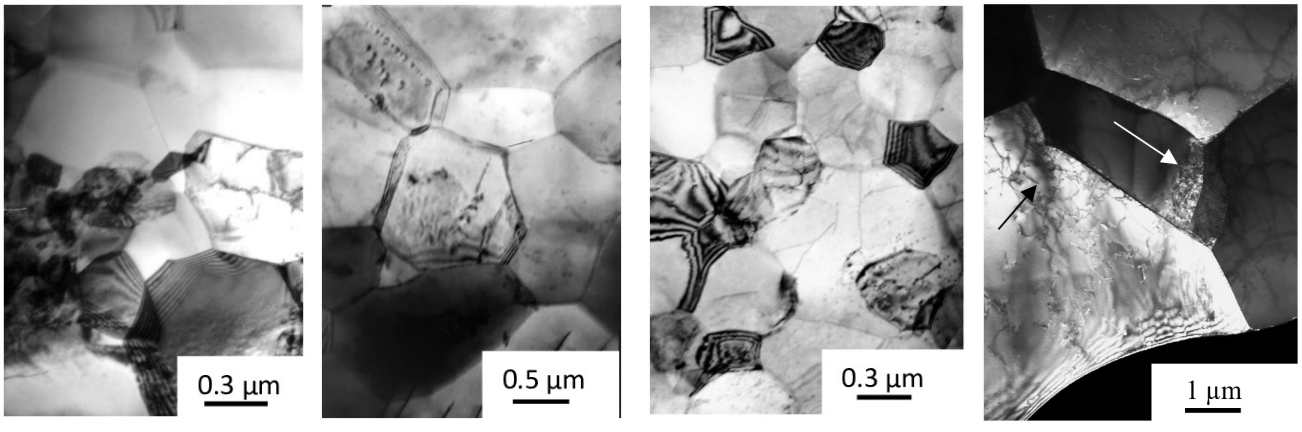

Fig. 3. Microstructure of iron after annealing at 523 (a), 723 (b), 823 (c), and 923 K (d): dark-field image in a $(110)_\alpha$ reflection. Arrows show dislocation pileups in the recrystallized grains. TEM.

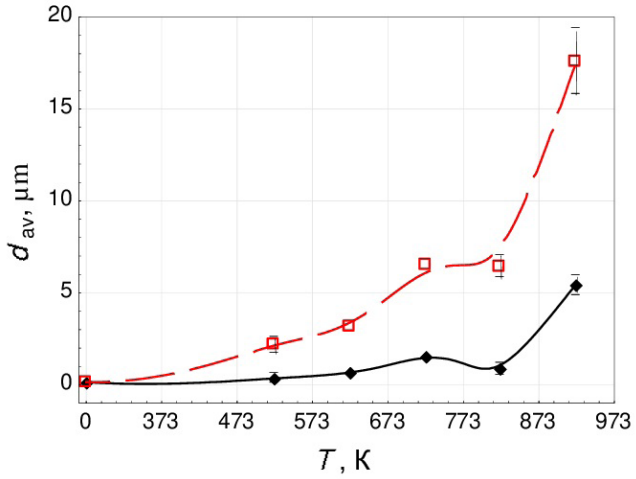

Fig. 4. (Color online) Average grain size according to (♦) TEM and (□) SEM examinations.

sample were also smaller than those located at a distance of 0.5–1 mm [11].

The grain size is seen to increase with increasing annealing temperature up to 723 K, then it remains unchanged after annealing at 823 K according to SEM data, while it decreases according to TEM data. These structural changes caused by annealing at 823 K may indicate the formation of additional thermally activated recrystallization centers at the boundaries that retained a nonequilibrium state [28]. A similar structural refinement was observed in a number of materials with an SMC structure upon annealing [11, 29, 30]. The formation of new grains increases the nonuniformity of the structure; EBSD analysis reveals grains with sizes greater than $5d_{av}$ (Table 1). This structure tends to secondary recrystallization upon subsequent heating [6, 31].

Annealing at 923 K increases the grain size significantly (Fig. 4, 3 d). The hardness did not change much (Fig. 2), but the fraction of the recrystallized structure, which was estimated using GOS, and the fraction of HABs (Table 1) decreased sharply. The TEM image (Fig. 3 d) shows dislocation pileups in the recrystallized grains. EBSD analysis can be used to estimate the density of geometrically necessary dislocations (GND): $\rho = \alpha\theta_{KAM}/(\mathbf{b}x)$, where α is the constant, **b** is the Burgers vector, x is the scanning step, and θ_{KAM} is the kernel average misorientation (KAM) determined as the average misorientation between a selected point and all its neighbors in the second coordinate sphere, rad. [32, 33]. Annealing at 923 K reduces the GND density to the greatest extent (Table 1). Analysis of changes in GOS, fraction of HABs, and dislocation density indicates the formation of a substructure in the grains at 923 K. Figure 5 shows a large number of LABs inside some grains. As a result, a peak appears at small angles in the misorientation angle distribution of the boundaries and the average grain misorientation angle decreases significantly (Table 1).

Figure 6 a shows inverse pole figures (IPFs) after annealing. These figures were obtained on the basis of the EBSD data at a bin size and Gaussian smoothing of 5°. The direction normal to the sample plane (ND) coincided with the axis of Bridgman anvil torsion. The texture of an axial <110> type is already observed after annealing at 523 K. Annealing at 723 K makes this textural component slightly weaker. However, a further increase in the annealing temperature makes the component much more pronounced. As a result, annealing at 823 and 923 K forms a pronounced recrystallization texture. The fraction of area occupied by grains with {110} planes (Fig. 6 b) that are parallel to the sample plane is about 60% and 90%, respectively, according to EBSD analysis. Grains of other orientations practically disappear after annealing at 923 K. The average grain misorientation angle decreases from 31° to 11° with increasing sharpness of the recrystallization texture (Table 1). A recrystallization texture forms during annealing of iron deformed by HPT at 300 K [34]. The intensification of the {110}<211> texture component during annealing at 873 K was observed in the Fe-Cr alloy deformed by HPT at room temperature [35, 36].

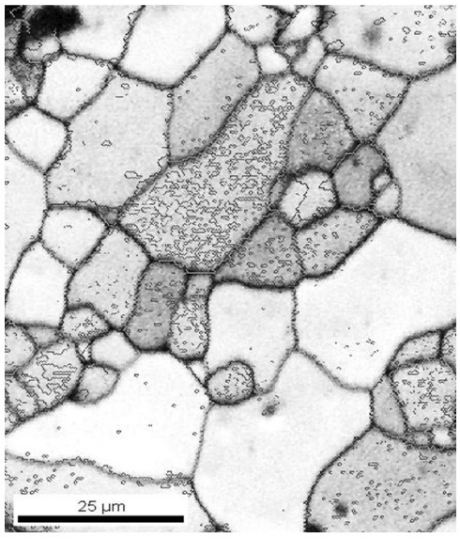

a

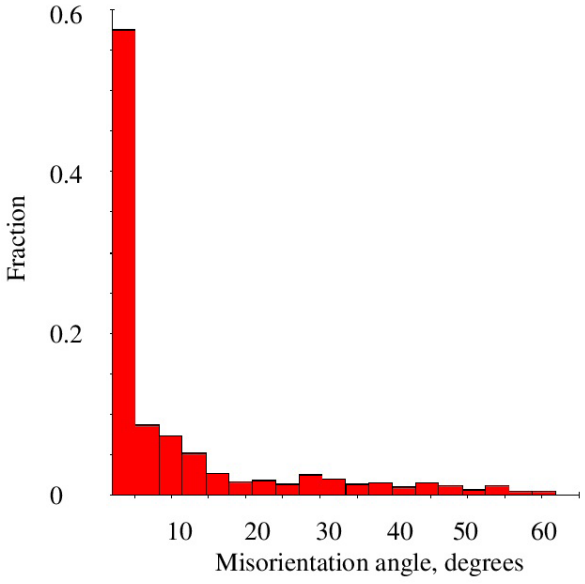

b

Fig. 5. Iron structure with the boundary scheme (a) and grain boundary misorientation histogram after deformation and annealing at 923 K for 1 h (b). HABs are in black, and LABs are in gray. EBSD data.

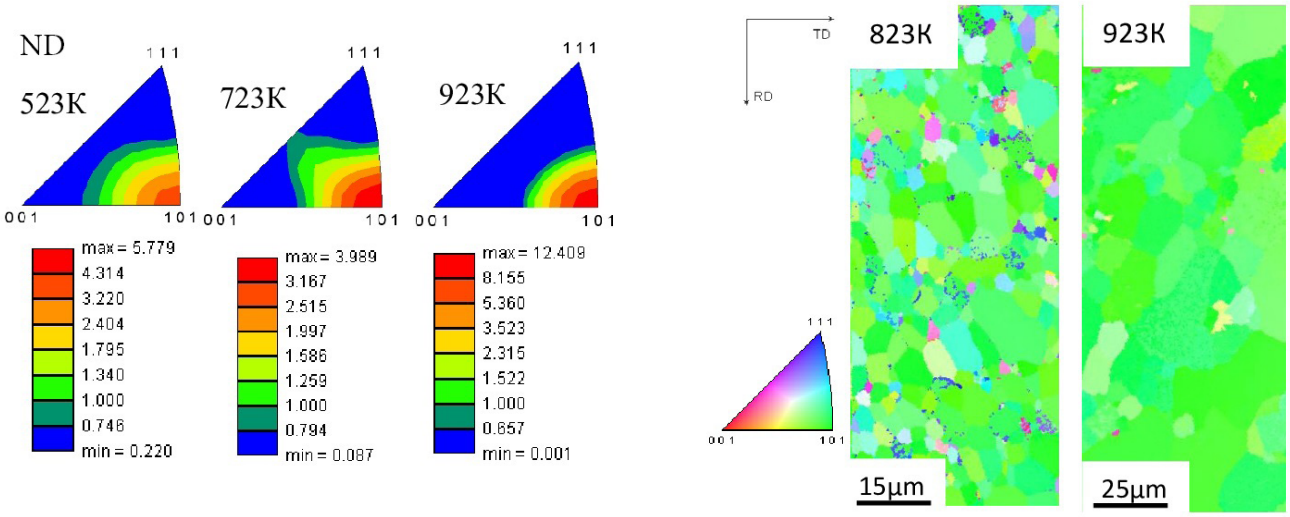

a b

Fig. 6. (Color online) Change in the microtexture upon annealing; IPFs after annealing at 523, 723, and 923 K (a) and orientation maps after annealing at 823 and 923 K (b).

Our study showed that a decrease in the deformation temperature to 80 K did not decrease the recrystallization temperature of the iron with SMC structure. After both cryogenic deformation and deformation at 300 K, recrystallization in iron develops considerably in 1 h at 523 K [34]. However, the size of the recrystallized grain after cryogenic deformation is larger than that after room-temperature deformation; in particular, the average grain size after annealing at 923 K is 18 and 2 μm, respectively [34]. The lower thermal stability of the structure formed during cryogenic deformation agrees with the data of other researchers [3,5]. The formation of a uniform-size grain structure at 523 – 723 K indicates the development of continuous recrystallization in this temperature range. The formation of thermally-activated recrystallization centers, the corresponding decrease in the average grain size, and the slight size heterogeneity at 823 K indicate that discontinuous and continuous recrystallization occur simultaneously. A similar phenomenon was observed in iron deformed at 300 K, but at a lower annealing temperature of 723 K [11, 34]. We should note that cryogenic deformation and annealing at 923 K greatly reduce the average grain misorientation angle to 11°. Its value after deformation at 300 K and similar annealing is not less than 25° [34]. Given that the {011}<100> recrystallization texture formed in both cases is close in sharpness, we can conclude about the existence of a more developed substructure in the case of recrystallization after cryogenic deformation. This fact is probably related to the rapid grain growth during the annealing due to the higher stored strain energy.

Therefore, the inhomogeneous SMC structure developed during cryogenic deformation does not affect the general patterns of recrystallization upon annealing.

4. Conclusions

The annealing behavior of pure iron with the SMC structure formed by high pressure torsion deformation at 80 K has been studied by SEM, TEM, and durometry techniques.

1. The hardness dependence on the sample radius observed after deformation (a greater distance from the center of the sample corresponds to a higher true strain and hardness) is maintained after annealing throughout the temperature range studied. The differences in hardness in different parts of the sample decrease with increasing temperature.
2. Annealing at 523 K significantly develops recrystallization (up to 90% of the material volume); the average grain size reaches 2 μm.
3. Recrystallization for 1 h is completed at 723 K and produces an equiaxed grain structure with an average grain size of 6.5 μm (according to SEM data).
4. Thermally activated recrystallization centers form at 823 K for 1 h. Analysis of the SEM data shows that the average grain size remains unchanged, while analysis of the TEM data shows that it decreases.
5. Annealing at 823 and 923 K forms the recrystallization texture of an axial <110> type. The average grain misorientation angle decreases from 31° to 11° with increasing sharpness of the recrystallization texture.
6. The recrystallized grains exhibit a substructure formed during annealing at 923 K in iron deformed at cryogenic temperature, which is not observed after the annealing of SMC iron deformed at room temperature.

Acknowledgments. This work was carried out within the state assignment themes "Pressure" 122021000032-5. The electron microscopic studies were per-formed at the Center of the Collaborative Access "Test Center of Nanotech-nologies and Advanced Materials," Institute of Metal Physics, Ural Branch, Russian Academy of Sciences.

References

1. K. Edalati, J. M. Cubero-Sesin, A. Alhamidi, I. F. Mohamed, Z. Horita. Mater. Sci. Eng. A. 613, 103 (2014). Crossref
2. A. V. Podolskiy, C. Mangler, E. Schafler, E. D. Tabachnikova, M. J. Zehetbauer. J. Mater. Sci. 48, 4689 (2013). Crossref

3. V. V. Popov, E. N. Popova, V. P. Pilyugin, D. D. Kuznetsov, A. V. Stolbovsky. IOP Conf. Series Mater. Sci. and Eng. 63, 012096 (2014). Crossref
4. V. V. Popov, E. N. Popova. Materials Transactions. 60, 1209 (2019). Crossref
5. V. V. Popov, E. N. Popova, D. D. Kuznetsov, A. V. Stolbovskii, V. P. Pilyugin. Phys. of Metals and Metallogr. 115, 682 (2014). Crossref
6. S. S. Gorelik. Recrystallization of Metals and Alloys. Moscow, MISIS (2005) 430 p. (in Russian)
7. T. Sakai, A. Belyakov, R. Kaibyshev, H. Miura, J. J. Jonas. Progress in Materials Science. 60, 130 (2014). Crossref
8. X. Wang, P. Li, K. Xue. Procedia Manufacturing 15, 1487 (2018). Crossref
9. N. A. Smirnova, V. I. Levit, V. P. Pilyugin, R. I. Kuznetsov, M. V. Degtyarev. Phys. Met. Metallogr. 62 (3), 140 (1986).
10. M. V. Degtyarev, L. M. Voronova, V. V. Gubernatorov, T. I. Chashchukhina. Doklady Physics, 47 (9), 647 (2002). Crossref
11. L. M. Voronova, M. V. Degtyarev, T. I. Chashchukhina. Phys. Metals Metallogr. 104 (3), 262 (2007). Crossref
12. Yu. V. Ivanisenko, A. A. Sirenko, A. V. Korznikov. Phys. Metals Metallogr. 87, 329 (1999).
13. A. A. Popov, I. Yu. Pyshmintsev, S. L. Demakov, A. G. Illarionov, R. Z. Valiev. Phys. Metals Metallogr. 83, 550 (1997).
14. A. P. Zhilyaev, T. G. Langdon. Progress in Materials Science. 53, 893 (2008). Crossref
15. J. Gubicza, N. Q. Chinh, E. Khosravi, S. V. Dobatkin, T. G. Langdon. Key Engineering Materials. 465, 195 (2011). Crossref
16. L. M. Voronova, T. I. Chashchukhina, M. V. Degtyarev. Phys. Metals Metallogr. 119, 969 (2018). Crossref
17. N. A. Smirnova, V. I. Levit, M. V. Degtyarev. Phys. Metals Metallogr. 66 (5), 185 (1988).
18. V. P. Pilyugin, L. M. Voronova, M. V. Degtyarev, T. I. Chashchukhina, V. B. Vykhodets, T. E. Kurennykh. Phys. Metals Metallogr. 110, 564 (2010). Crossref
19. M. V. Degtyarev, L. M. Voronova, T. I. Chashchukhina. Russian Metallurgy (Metally). 2005 (5), 390 (2005).
20. L. M. Voronova, M. V. Degtyarev, T. I. Chashchukhina. Phys. Metals Metallogr. 109, 135 (2010). Crossref
21. H. W. Zhang, X. Huang, R. Pippan, N. Hansen. Acta Materialia. 58, 1698 (2010). Crossref
22. H. H. Bernardi, H. R. Z. Sandim, K. D. Zilnyk, B. Verlinden, D. Raabe. Materials Research. 20 (5), 1238 (2017). Crossref
23. F. J. Humphreys. J. Mater. Sci. 36 (16), 3833 (2001). Crossref
24. S. A. Saltykov. Stereometric Metallography. Moscow, Metallurgiya (1976) 270 p. (in Russian)
25. J.-l. Ning, E. Courtois-Manara, L. Kurmanaeva, A. V. Ganeev, R. Z. Valiev, Ch. Kübel, Yu. Ivanisenko. Mater. Sci. and Eng. A. 581, 8 (2013). Crossref
26. D. P. Field, L. T. Bradford, M. M. Nowell, T. M. Lillo. Acta Mater. 55, 4233 (2007). Crossref
27. A. Yu. Eroshenko, Yu. P. Sharkeev, M. A. Khimich, I. A. Glukhov, P. V. Uvarkin, A. I. Tolmachev, A. M. Mairambekova. Lett. on Mater. 10 (1), 54 (2020). (in Russian) Crossref
28. V. N. Perevezentsev, A. S. Pupynin, A. E. Ogorodnikov. Lett. on Mater. 9 (1), 107 (2019). Crossref
29. L. M. Voronova, M. V. Degtyarev, T. I. Chashchukhina. Phys. Metals Metallogr. 122, 559 (2021). Crossref
30. M. Degtyarev, T. Chashchukhina, L. Voronova, T. Gapontseva, V. Levit. International Journal of Refractory Metals & Hard Materials. 86, 105117 (2020). Crossref
31. V. Yu. Novikov. Secondary recrystallization. Moscow, Metallurgy (1990) 128 p. (in Russian)
32. C. Moussa, M. Bernacki, R. Besnard, N. Bozzolo. IOP Conf. Series: Mater. Sci. and Eng. 89, 012038 (2015). Crossref
33. M. Calcagnotto, D. Ponge, E. Demir, D. Raabe. Mater. Sci. and Eng. A. 527, 2738 (2010). Crossref
34. L. M. Voronova, M. V. Degtyarev, T. I. Chashchukhina, D. V. Shinyavskii, T. M. Gapontseva. Lett. on Mater. 7 (4), 359 (2017). Crossref
35. J. Duana, H. Wen, C. Zhou, R. Islamgaliev, X. Li. Materialia. 6, 100349 (2019). Crossref
36. J. Duan, H. Wen, C. Zhou, X. He, R. Islamgaliev, R. Valiev. J. Mater. Sci. 55,7958 (2020). Crossref